# Edinburgh Research Explorer

# Non-invasive detection of ischemic vascular damage in a pig model of liver donation after circulatory death

# Noninvasive Detection of Ischemic Vascular Damage in a Pig Model of Liver Donation After Circulatory Death

Katherine J.I. Ember (iD),[1] Fiona Hunt,[2] Lauren E. Jamieson,[3] John M. Hallett,[4] Hannah Esser,[4] Timothy J. Kendall (iD),[5,6] R. Eddie Clutton,[7] Rachael Gregson,[7] Karen Faulds,[3] Stuart J. Forbes (iD),[4] Gabriel C. Oniscu,[2,8*] and Colin J. Campbell[1*]

**BACKGROUND AND AIMS:** Liver graft quality is evaluated by visual inspection prior to transplantation, a process highly dependent on the surgeon's experience. We present an objective, noninvasive, quantitative way of assessing liver quality in real time using Raman spectroscopy, a laser-based tool for analyzing biomolecular composition.

**APPROACH AND RESULTS:** A porcine model of donation after circulatory death (DCD) with normothermic regional perfusion (NRP) allowed assessment of liver quality premortem, during warm ischemia (WI) and post-NRP. Ten percent of circulating blood volume was removed in half of experiments to simulate blood recovery for DCD heart removal. Left median lobe biopsies were obtained before circulatory arrest, after 45 minutes of WI, and after 2 hours of NRP and analyzed using spontaneous Raman spectroscopy, stimulated Raman spectroscopy (SRS), and staining. Measurements were also taken *in situ* from the porcine liver using a handheld Raman spectrometer at these time points from left median and right lateral lobes. Raman microspectroscopy detected congestion during WI by measurement of the intrinsic Raman signal of hemoglobin in red blood cells (RBCs), eliminating the need for exogenous labels. Critically, this microvascular damage was not observed during WI when 10% of circulating blood was removed before cardiac arrest. Two hours of NRP effectively cleared RBCs from congested livers. Intact RBCs were visualized rapidly at high resolution using SRS. Optical properties of ischemic livers were significantly different from preischemic and post-NRP livers as measured using a handheld Raman spectrometer.

**CONCLUSIONS:** Raman spectroscopy is an effective tool for detecting microvascular damage which could assist the decision to use marginal livers for transplantation. Reducing the volume of circulating blood before circulatory arrest in DCD may help reduce microvascular damage. (HEPATOLOGY 2021;0:1-16).

Liver disease is a growing global burden, and transplantation is the only life-saving treatment. However, the number of donor organs available for transplantation is insufficient to meet the rising demand. In the United States alone, 12,000 patients are currently waiting for a liver transplant, while 1,700 people died before receiving a transplant in 2013.[1,2] Despite the medical community's best efforts, around 20% (approximately 1,300) of the liver recovered each year in the United States are not transplanted, which almost matches the number of waiting list deaths.[3,4] The high discard rate is partly due to uncertainty about viability and posttransplant

function. Currently, liver quality is evaluated based on donor past medical history, liver biochemistry at time of death, and appearance as judged subjectively by the operating surgeon. Therefore, a quantitative and dynamic system of assessing liver health in real time would be invaluable.

Although donation after brain death is predominant in many countries, in recent years there has been an increasing reliance upon donation after circulatory death (DCD).[4] During the DCD pathway, multiple factors can affect liver viability; therefore, it is particularly important for surgeons to be able to assess the liver health. After circulatory arrest, the body undergoes a variable period of limited blood supply known as warm ischemia (WI). Restricted oxygen and nutrient availability causes organs to enter a hypoxic state, accompanied by a metabolic switch from aerobic to anaerobic respiration. Extended WI is detrimental to posttransplant function.[5,6] In the DCD setting, WI is followed by cold perfusion of the organs and storage on ice prior to transplantation. However, a technique called normothermic regional perfusion (NRP) breaks this cycle. NRP uses an extracorporeal circuit to pump oxygenated blood around isolated abdominal organs *in situ* at body temperature (37°C). This allows recovery from WI before the cold perfusion step and has led to promising results in terms of organ use and outcomes.[7,8] Moreover, as blood circulation to the organ is restored, NRP provides an opportunity for a dynamic assessment of liver function and biochemistry. Despite such recent advances in transplant technology, there are few well-characterized methods for assessment or prediction of liver function in a rapid, noninvasive manner.

One sensing technology that could provide such information is spectroscopy. Spectroscopic techniques use electromagnetic radiation (light) to detect and identify molecules by virtue of their molecular structure. Among these techniques, Raman spectroscopy uses nonionizing radiation to yield specific molecular information. Laser light is directed at a sample, where it induces energetic transitions. As energy levels depend on the precise molecular structure, the inelastically (Raman) scattered light contains information specific to the molecules within the sample, providing a unique "spectroscopic fingerprint."[9-11] This scattered light can be passed through a series of optics onto a detector using a spectrometer.

A Raman spectrum plots wave number (inversely proportional to wavelength) against intensity of Raman scattering. The rapid energetic transitions involved in Raman scattering result in narrow peaks at specific wave numbers. These contrast with the broad peaks of fluorescence, which can span hundreds of wave numbers. Although fluorescence spectroscopy is a better-established technique in biomedicine, the fluorescence profile of one molecule can easily overlap with another, leading to low molecular specificity. Moreover, while fluorescence spectroscopy often employs exogenous fluorophores, Raman can be used in a label-free manner.

Many analytical chemical techniques require biopsies for testing. Raman spectroscopy, however, has the potential to give information about the biomolecular state of cells or organs *in situ*, maintaining sample integrity. This renders it extremely useful for primary research, disease diagnosis, and monitoring repair. Raman technology has evolved rapidly in recent years and can be incorporated into a relatively inexpensive portable device for point-of-care use or a microscope for high-resolution imaging of biopsies or live cells.

## ARTICLE INFORMATION:

From the [1]Department of Chemistry, University of Edinburgh, Edinburgh, United Kingdom; [2]Edinburgh Transplant Centre, Royal Infirmary of Edinburgh, Edinburgh, United Kingdom; [3]Technology and Innovation Centre, University of Strathclyde, Glasgow, United Kingdom; [4]Centre for Regenerative Medicine, University of Edinburgh, Edinburgh, United Kingdom; [5]Edinburgh Pathology Department, The Royal Infirmary of Edinburgh, United Kingdom; [6]University of Edinburgh Centre for Inflammation Research, Edinburgh, United Kingdom; [7]Roslin Institute, University of Edinburgh, Edinburgh, United Kingdom; [8]Department of Clinical Sciences, University of Edinburgh, Edinburgh, United Kingdom.

## ADDRESS CORRESPONDENCE AND REPRINT REQUESTS TO:

Colin J. Campbell, B.Sc.(Hons), Ph.D.                     E-mail: colin.campbell@ed.ac.uk
Department of Chemistry, University of Edinburgh          Tel.: 44 (0)131 651 3049
Edinburgh, UK

It has been used in multiple biomedical applications,[12] from discriminating between cell types[13,14] to detection of invasive brain cancer during surgery in real time.[15] However, a Raman spectroscopic tool for detecting liver damage in the clinic has yet to be developed. We explored whether Raman can yield meaningful information to assist the evaluation of liver grafts.

Our hypothesis was that Raman spectroscopy could be used to discriminate between healthy, damaged, and recovered liver tissue by detecting molecular changes within the tissue. To determine whether this was possible in a clinical setting, we used a porcine DCD model incorporating a period of WI followed by NRP. As DCD heart transplantation is increasing, we also explored the impact of blood removal (current clinical practice to enable donated heart preservation). Therefore, we implemented alterations to half of the surgical procedures by reducing the circulating volume of blood prior to circulatory arrest.

We used three different forms of Raman spectroscopy in our analyses: (1) spontaneous Raman spectroscopy of biopsies using a Raman microscope (this yielded information about the whole Raman spectrum); (2) stimulated Raman scattering (SRS) microscopy to image biopsies at high resolution within seconds, determining the precise source of Raman signal; and (3) a handheld Raman spectrometer to collect optical information from *in situ* intact livers.

To substantiate our findings, we employed a variety of complementary techniques including blood gas analyses for systemic chemical information, hematoxylin and eosin (H&E) stains for microscopic data about morphological changes, and 3,3′-diaminobenzidine (DAB) stains for more targeted histological information. Although this paper focuses on NRP, the same technology could be applied to evaluate livers during *ex situ* normothermic machine perfusion.

# Materials and Methods

## PORCINE MODEL OF DCD

We used a porcine model of DCD with NRP for a number of reasons. Firstly, pig liver is similar in size and structure to human liver. Secondly, the model includes an extended period (45 minutes) of WI, defined as the time between circulatory arrest

and perfusion. Thirdly, NRP recirculates oxygenated blood to abdominal organs and thus potentially restores the organs close to their preischemic status (Fig. 1A).

All animal work was approved by the Animal Welfare and Ethical Review Committee of the Roslin Institute, and the work was conducted under Home Office (UK) Licence PPL: PF5151DAF 130418. Female pigs weighing 50-60 kg (n = 12) were anesthetised, heparinized, ventilated, and monitored using a central line and electrocardiogram. A laparotomy was carried out, and initial spectral readings were acquired. Liver biopsies were taken. Circulatory arrest was induced with KCl injection, and after a short agonal phase (1-8 minutes, mean time = 3 minutes), cardiac arrest timing was recorded. Livers underwent 45 minutes of WI, followed by 2 hours of NRP using Donor Assist (Organ Assist, Groningen, the Netherlands) or Maquet Rotaflow (Maquet; Gettinge, Rastatt, Germany). As only pigs 9 and 10 were perfused using the Maquet Rotaflow, a comparison between the two NRP machines could not be made with meaningful statistical power. However, pigs 9 and 10 did not yield anomalous results. During NRP, the abdominal aorta and vena cava were cannulated and connected to the extracorporeal circuit. The supradiaphragmatic aorta was clamped prior to starting perfusion, preventing brain perfusion. The pump priming fluids, the vascular cannulae, and the perfusion parameters were maintained irrespective of the device used. These were similar to clinical practice and have been published elsewhere.[7]

In seven pigs (blood withdrawal group), 10% of the circulatory volume was removed 1-2 hours prior to cardiac arrest to mimic blood removal for DCD heart procurement and preservation and assess impact on the conduct of abdominal NRP. No blood was removed from pigs 9-12 (constant blood group, n = 4) in keeping with current abdominal NRP organ retrieval process. Pig 1 was a trial run in which the handheld Raman spectrometer did not function until NRP120, so these results were not included.

## SAMPLE COLLECTION AND PREPARATION

Liver biopsies were taken at three time points: prior to cardiac arrest (T0), after 45 minutes of

**A**



**B**
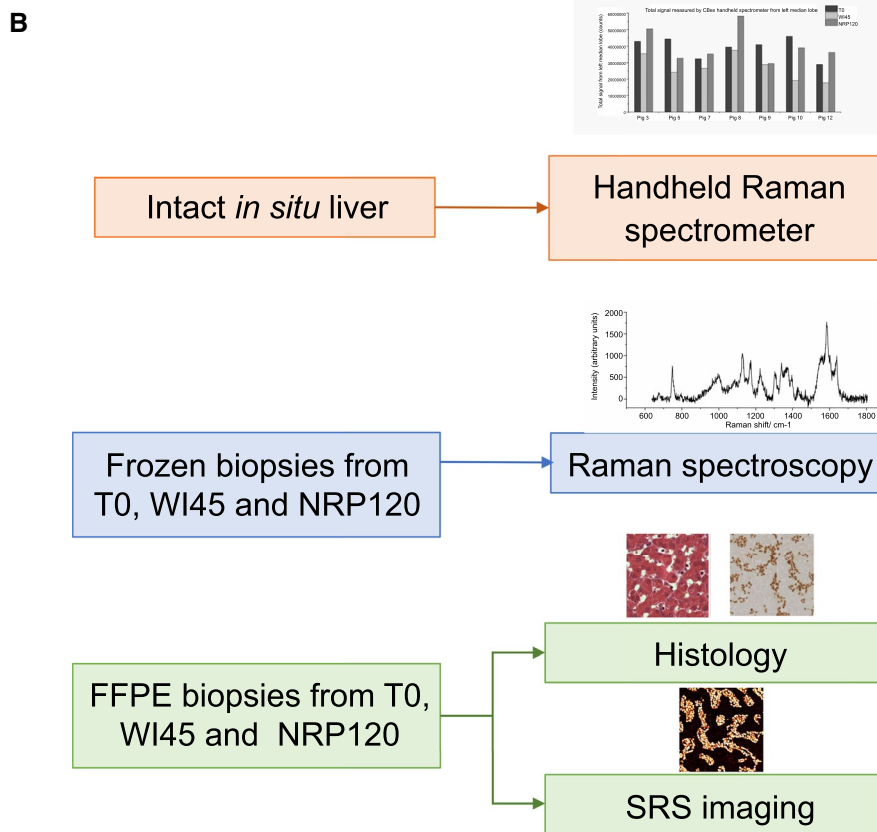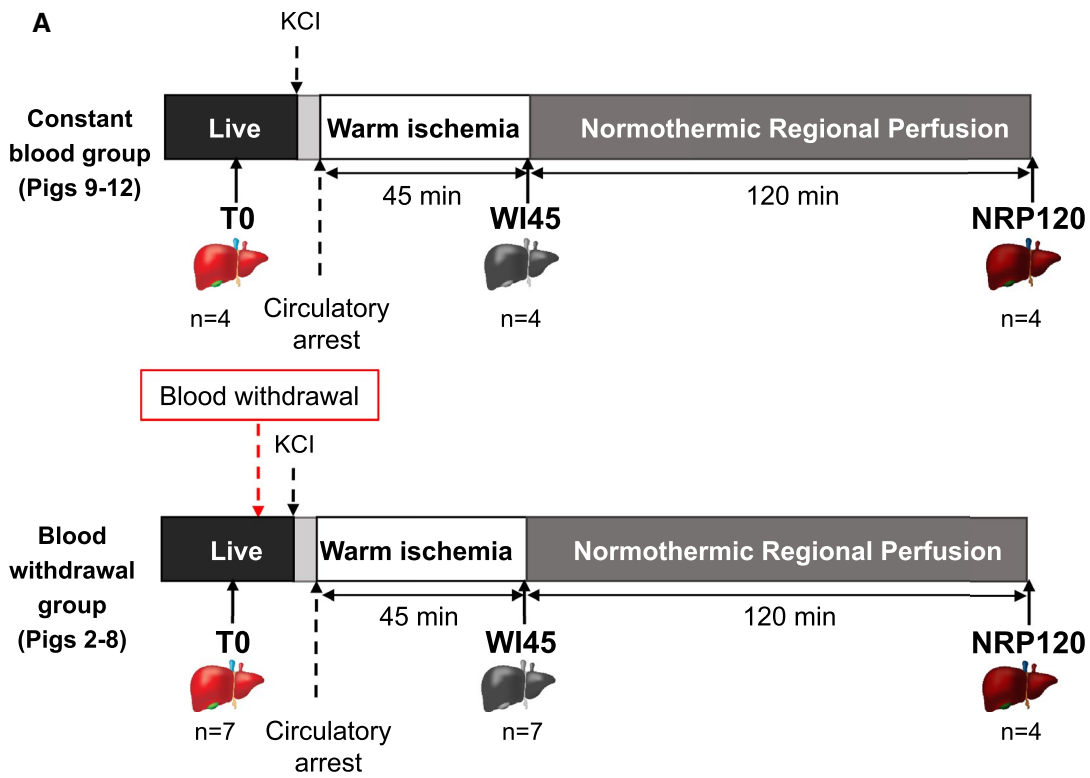
FIG. 1. Illustration of experimental model. (A) Schematic of porcine model of donation after circulatory death. In the constant blood group, no blood was removed. In the blood withdrawal group, 10% of the circulating volume of blood was removed prior to circulatory arrest. T0, n = 11; WI45, n = 11; NRP120, n = 8 (as pigs 2, 4, and 6 were not NRP-perfused due to time constraints). (B) Experimental workflow showing samples taken and experimental analyses carried out. Abbreviation: FFPE, formalin-fixed, paraffin-embedded.

WI (WI45), and after 2 hours of NRP (NRP120) (Fig. 1A). Blood and perfusate (4 mL) were taken at T0 and NRP120, respectively. Two biopsies were taken from the left median lobe (LML) of the liver (approximately 0.125 cm$^3$): one frozen on dry ice and one fixed in 4% formalin. Formalin-fixed samples were stored in 70% ethanol after 12 hours of fixation. Blood samples were collected in K2EDTA tubes and spun for 5 minutes at 1,500 RCF. Resulting cell fractions were snap-frozen. Formalin-fixed samples were paraffin-embedded and sectioned to 4 µm thickness onto glass slides for staining and SRS spectroscopy (Fig. 1B).

For Raman microspectroscopy, frozen tissue samples were sectioned to 7 µm thickness in a –20°C cryostat and mounted onto Raman-grade calcium fluoride windows. Samples were frozen at –4°C and thawed at room temperature for 20-40 minutes before spectral acquisition.

## BLOOD GAS AND LIVER BIOCHEMISTRY MEASUREMENTS

Blood was drawn for blood gas analysis and biochemistry analysis, confirming that the DCD time course produced measurable changes in liver biochemistry (see Supporting Fig. S1 and Table S1).

## HISTOLOGY

The H&E staining protocol is detailed in the Supporting Material. H&E-stained slides were graded on the Suzuki scale using congestion, vacuolization, and necrosis as parameters by a trained, dedicated liver pathologist who was blinded to samples.[16] These categorical data were plotted as scatter plots rather than box-and-whisker plots. To count red blood cells (RBCs) present in liver parenchyma sections, formalin-fixed sections were DAB-stained (coloring RBCs brown due to endogenous peroxidase activity). Slides were imaged using a Zeiss Axio Scan Z.1 slide scanner (Zeiss, Oberkochen, Germany) and images analyzed using QuPath open source tissue

analysis software[17] (P. Bankhead). RBCs were quantified using QuPath semiautomated cell detection, and total tissue area was determined using the tissue detection tool.

## RAMAN MICROSPECTROSCOPY

Raman spectral maps of liver parenchyma cryosections on calcium fluoride discs were taken using a Renishaw InVia Raman microspectrometer (Renishaw Plc, New Mills, Wotton-under-Edge, Gloucestershire, UK). Spectral maps were obtained at spectral regions spanning 600-1,800 cm$^{-1}$ with 50-µm step sizes in the $x$ and $y$ directions using a 532 nm laser at 6.8 mW power with a ×20 objective. Each spectrum was acquired with a 2-second acquisition time. Raman spectra were acquired from pure bovine hemoglobin crystals at 0.6 mW laser power, ×20 objective, 5-second acquisition with six accumulations. Frozen blood samples were thawed and air-dried for 20 minutes, and spectral measurements were acquired. Spectra of dried blood samples on calcium fluoride discs were taken in the same manner, and an average of six spectra was used as a representative blood spectrum.

## RAMAN DATA PROCESSING

Spectra were preprocessed in Wire 4.1 software: cosmic rays were removed and raw spectra baseline-corrected to remove background fluorescence signal using a third-order polynomial (Supporting Fig. S2). Mean spectra from maps were plotted in MATLAB 2017a. False-color maps in Wire 4.1 were created using direct classical least squares (DCLS), which measure the spectral fit to the reference spectrum, using the spectrum of hemoglobin as a reference. Lookup table values were set from 0.5 to 1 and converted to gray scale and regions of interest (ROI) assigned from comparison to brightfield images of the tissue cryosection. The number of pixels above a threshold gray-scale value of 100 were counted as a percentage of the total ROI pixel area.

## SRS MICROSPECTROSCOPY

SRS images were obtained using a Leica Microsystem SP8 multiphoton confocal microscope with a ×25/NA 0.95 HC PL water immersion objective and a CARS 1200S filterwheel. Data were acquired using a 100-mW Stokes (1,032 nm excitation) and a 200-mW pump laser (886.6 nm excitation), which excited the 1,585-cm$^{-1}$ peak (peak vibration of hemoglobin). The pump laser was also tuned to 894.1 nm to excite a vibration at 1,490 cm$^{-1}$ (a region with low signal from hemoglobin, taken to be background) (Supporting Fig. S3). Signal was detected in transmission mode on a photomultiplier tube detector. Images were acquired with a 227.3 gain, 1,024 × 1,024 resolution, and a line average of 5.

## HANDHELD AUTOFLUORESCENCE MEASUREMENTS

Spectra were measured between 400 and 2,300 cm$^{-1}$ using a 785-nm excitation handheld CBex Raman spectrometer (Snowy Range Instruments, Laramie, WY) with a 10-second acquisition time and 10.8 mW laser power. A plastic sheath with no detectable Raman scattering was used to protect the lens and maintain sterility while the objective lens was pressed against the liver surface. This was changed between measurements (Supporting Fig. S4).

Readings were taken from the LML and right lateral lobe *in situ* at T0, WI45, and NRP120. For total intensity, the sum of the signal from 400 to 2,300 cm$^{-1}$ was taken (Supporting Fig. S5). The effects of a number of environmental factors (environmental light, movement during ventilation) were also measured (Supporting Figs. S6 and S7) and found to have no statistically significant effect on readings.

## STATISTICS

All graphs were plotted in Origin (OriginLab, Northampton, MA), and statistical analysis was undertaken using IBM SPSS Statistics Software. For nonparametric data, a Mann-Whitney test was used to determine significance. For paired data with more than two measurements, repeated measures ANOVA was used for parametric data and Friedman's test for nonparametric data. Wilcoxon's signed rank test was used for nonparametric paired data. For categorical data, a chi-squared test was used with exact significance. In all cases, $P < 0.05$ was taken to be significant.

# Results

## LIVER PATHOLOGY INDICATES ISCHEMIC CONGESTION IS RELIEVED WITH REDUCED BLOOD VOLUME

H&E stains showed that RBCs accumulated in the liver parenchyma sinusoids during WI in the group with a constant blood volume (constant blood group; Fig. 2A), suggesting that microvascular damage has occurred during WI. These RBCs were cleared to varying degrees by NRP120. This level of congestion was not observed at any time point in animals which had 10% circulating volume removed before circulatory arrest (blood withdrawal group; Fig. 2B), apart from pig 5 which had anomalous blood gas measurements (see Supporting Table S1).

A trained pathologist blinded to the identity of H&E liver biopsy samples scored them according to congestion, necrosis, and vacuolization; and these were combined into an overall Suzuki score for liver damage. Preischemic liver morphology was normal in all animals, as visualized by H&E (Fig. 2A,B), including those with no NRP120 time point (Supporting Fig. S8). At T0, there was either no congestion or minimal congestion in all animals (Fig. 2C,D) and overall Suzuki scores indicated minimal damage (Fig. 2E-G).

At WI45, there were marked histological differences between the constant blood group and the blood withdrawal group. In the constant blood group, severe congestion was apparent at WI45 (Fig. 2A), and pathologist congestion scores were significantly worse at WI45 compared to T0 and NRP120 (Fig. 2C). The same was true for the Suzuki score (Fig. 2E), suggesting that liver damage occurred during ischemia and was relieved by NRP. However, necrosis and vacuolization scores remained unchanged (Supporting Fig. S9A,C).

Conversely, the extent of congestion was much less severe during WI in the blood withdrawal group (Fig. 2B; Supporting Fig. S8). There was no
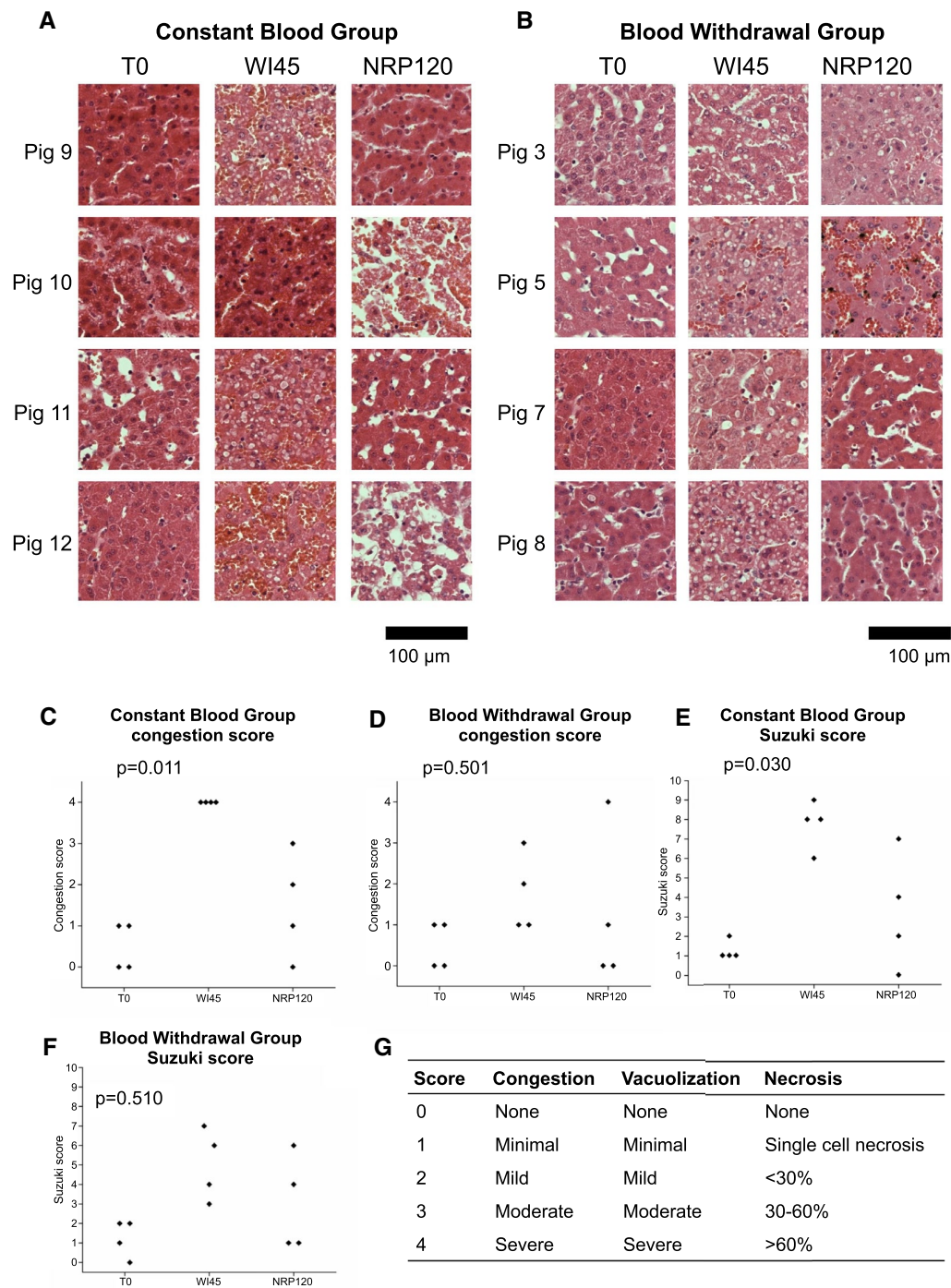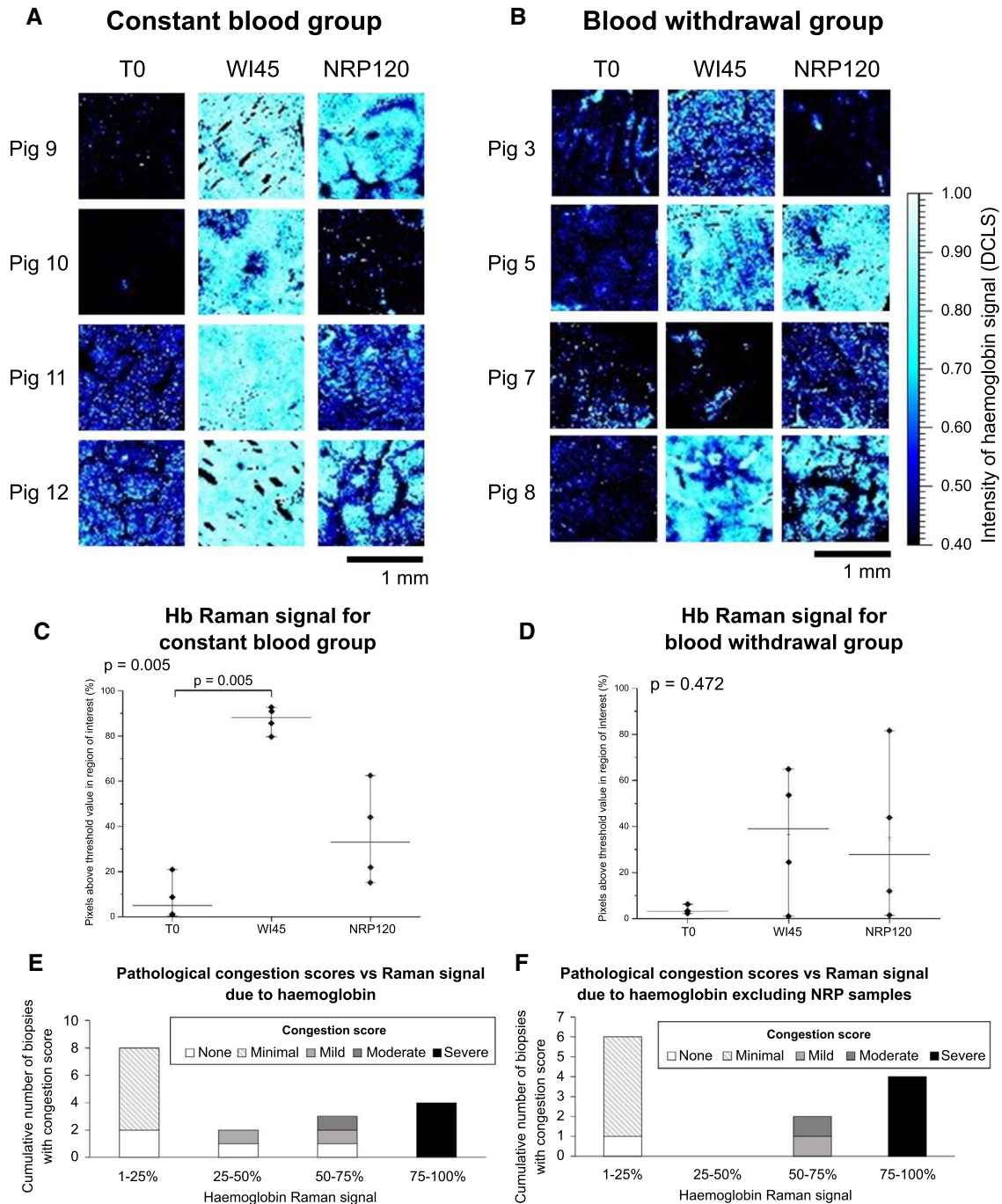
**FIG. 2.** Histological analysis of porcine liver parenchyma at T0, WI45, and NRP120 in the constant blood and blood withdrawal groups. (A,B) H&E stains. (A) In the constant blood group, blood volume was constant. (B) The blood withdrawal group had 10% of circulating blood removed before circulatory arrest. (C-F) Pathological scoring of formalin-fixed, paraffin-embedded liver sections by a trained pathologist. (C) Constant blood group congestion scores are significantly higher at WI45 ($\chi^2[12] = 16.000$, $P = 0.011$). (D) Blood withdrawal group congestion scores are not significantly different across the time course ($\chi^2[12] = 8.400$, $P = 0.501$). (E,F) Suzuki score for liver damage in constant blood group and blood withdrawal group animals. (E) Constant blood group Suzuki scores are significantly higher at WI45 ($\chi^2[12] = 21.000$, $P = 0.030$). (F) Blood withdrawal group Suzuki scores are not significantly different across the time course ($\chi^2[12] = 14.000$, $P = 0.510$). (G) Suzuki scoring system for liver damage.[16] In the Suzuki scoring system, liver sections are given scores associated with congestion, vacuolization, and necrosis. These are added to give an overall Suzuki score for liver damage encompassing these factors.

significant difference between congestion, Suzuki, necrosis, and vacuolization scores across the time course (Fig. 2D,F; Supporting Fig. S9B,D). These results strongly indicate that reducing blood volume before circulatory arrest may reduce liver congestion and damage.

In all pigs, NRP120 congestion scores were comparable to T0 scores, suggesting that NRP can alleviate liver congestion. However, a notable exception was pig 5 in the blood withdrawal group. In this case, erythrocytes accumulated at WI45 and continued to do so during NRP. This animal had abnormal blood gas measurements at T0, with aspartate aminotransferase of 904 U/L (see Supporting Table S1), suggesting that prolonged liver congestion is associated with biochemical damage.



**A** Constant blood group

**B** Blood withdrawal group

**C** Hb Raman signal for constant blood group

**D** Hb Raman signal for blood withdrawal group

**E** Pathological congestion scores vs Raman signal due to haemoglobin

**F** Pathological congestion scores vs Raman signal due to haemoglobin excluding NRP samples

**FIG. 3.** Raman maps of liver parenchyma at T0, WI45, and NRP120 in the constant blood and blood withdrawal groups. (A,B) Raman maps of hemoglobin signal in 7-μm-thick porcine liver parenchyma cryosections. (A) In the constant blood group, blood volume was constant. (B) The blood withdrawal group had 10% of the circulating volume of blood removed before circulatory arrest. Color bar corresponds to hemoglobin signal intensity using DCLS and pure hemoglobin crystals as a reference. Spectral maps were obtained at spectral regions spanning 600-1,800 cm$^{-1}$ with 50-μm step sizes in the $x$ and $y$ directions using a 532-nm laser at 6 mW power with a ×20 objective. Each spectrum was acquired with a 2-second acquisition time and baseline-corrected. All samples were mounted on calcium fluoride discs. (C,D) Box-and-whisker plots of hemoglobin signal from liver parenchyma Raman maps. Percentage of pixels above a threshold value within an ROI comprising the whole cryosection were measured from maps of hemoglobin signal (from DCLS). Threshold gray value was set at 100. (C) In the constant blood group, the hemoglobin Raman signal at WI45 was significantly greater than at T0 or NRP120 (Friedman's test ($\chi^2$[2] = 8.000, $P$ = 0.005, n = 4). (D) In the blood withdrawal group, there was no statistically significant difference across the time course ($\chi^2$[2] = 1.500, $P$ = 0.472, n = 4). (E,F) Relation between pathological congestion scores and Raman signal due to hemoglobin in porcine liver biopsies (E) in all samples and (F) excluding NRP samples. A stronger correlation between congestion score and hemoglobin signal is observed when NRP samples are excluded. Livers were scored for congestion on a scale of "none" to "severe" by a trained pathologist.

## RAMAN SPECTRAL MAPPING DETECTS CONGESTION IN A STAIN-FREE MANNER

We detected erythrocytes in congested ischemic biopsies in a label-free way due to the intrinsic Raman signal of hemoglobin using a 532-nm excitation laser.

The Raman signal apparent in parenchyma was almost entirely due to hemoglobin, indicated by the high degree of similarity to Raman spectra of pure hemoglobin crystals and red blood fractions (Supporting Fig. S10). To verify whether we could use this signal to measure RBC accumulation, we obtained Raman maps from parenchyma cryosections across the DCD time course. Each pixel represents a spectrum acquired from one point on the section. By raster-scanning the laser spot across the sample, Raman microspectroscopy can be used to plot the distribution of molecules based on their molecular signature. Certain regions of the parenchyma cryosections had a strong Raman spectrum primarily composed of peaks from hemoglobin (Supporting Fig. S10). The remainder of the tissue exhibited low Raman signal and high background fluorescence (see pig 12 T0 spectra in Supporting Fig. S2). We created false-color Raman maps of parenchyma sections where pixel intensity is proportional to the intensity of the hemoglobin signal, determined by DCLS (Fig. 3A,B). To quantify the hemoglobin signal within a cryosection, we measured the percentage of pixels above a threshold hemoglobin signal intensity in a ROI of approximately 4 × 4 mm in area (Fig. 3C,D).

The hemoglobin signal in WI45 tissue was significantly greater than at T0 or NRP120 in the constant blood group (Fig. 3A,C). Conversely, there was no significant difference in hemoglobin signal across the time course in the blood withdrawal group (Fig. 3B,D; Supporting Fig. S11). Figure 3E,F shows a correlation between pathological congestion scores and hemoglobin Raman signal. All biopsies with severe congestion (congestion score = 4) had a hemoglobin signal intensity of >79% (pixels above threshold value), while all biopsies with no to moderate congestion (congestion scores 0-3) had a hemoglobin signal intensity of <70%. A threshold signal intensity could assist in discriminating between severely congested samples and livers with free hemoglobin present.

When NRP120 results were excluded (Fig. 3F), the correlation became stronger, with all noncongested or minimally congested samples having a hemoglobin signal intensity of 0-25%, all mildly to moderately congested samples having a signal intensity of 50%-75% and all severely congested samples having a signal intensity of >75%. This may be because free hemoglobin is present in the liver after RBCs (the measure of congestion) have been broken down

## UNLABELED RAMAN MAPS CORRELATE WITH RBCs VISUALIZED USING DAB STAINING

As an independent quantitative measure of RBC accumulation, we stained RBCs brown using DAB (Fig. 4A,B). Semiautomated quantification showed that there were significantly more RBCs in ischemic tissue from constant blood group animals than blood
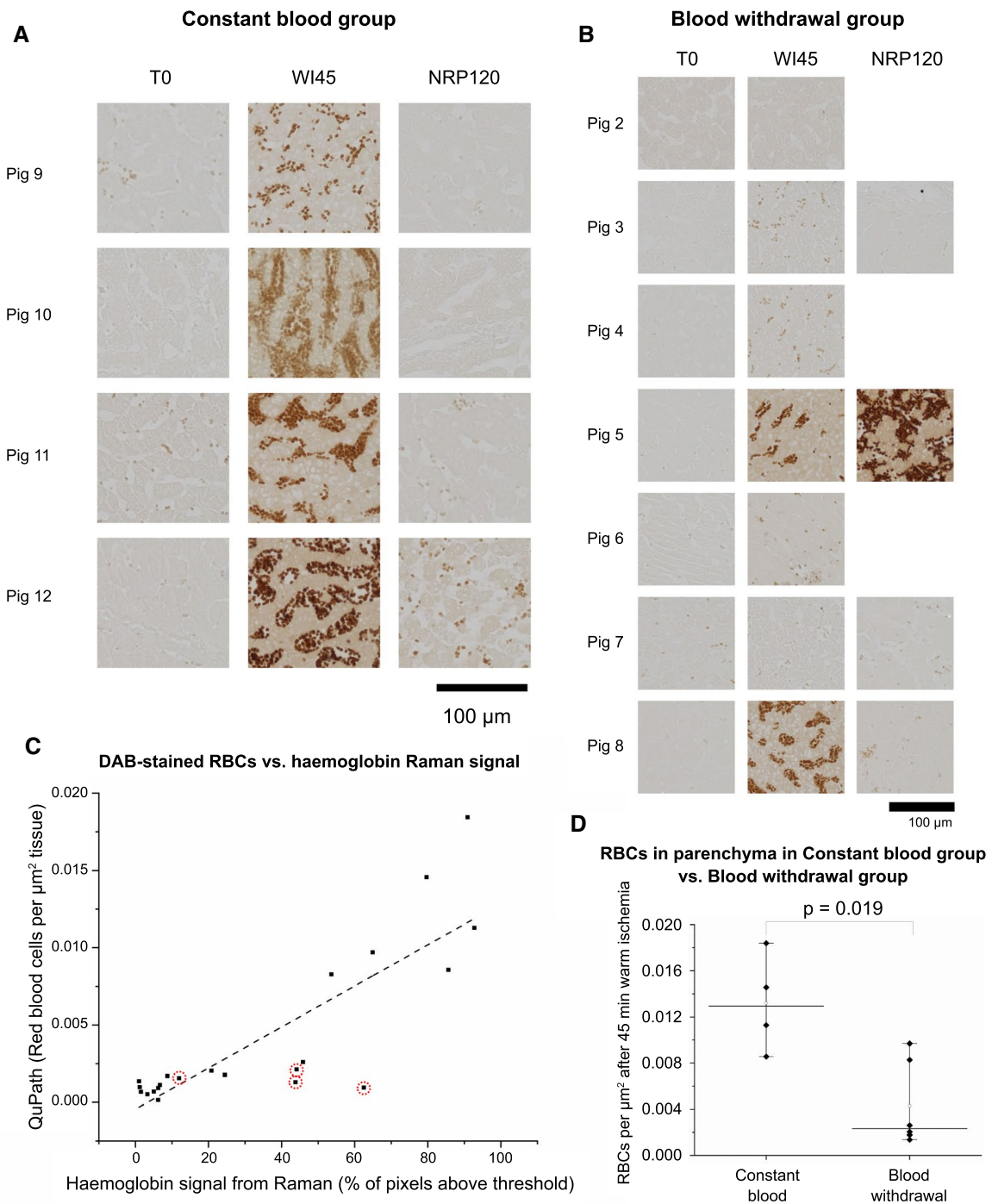
**FIG. 4.** DAB-stained liver parenchyma from T0, WI45, and NRP120 biopsies. RBCs are stained brown. (A) In the constant blood group, blood volume was constant. (B) The blood withdrawal group had 10% of circulating volume of blood removed prior to circulatory arrest. (C) Scatter plot of hemoglobin signal measured using Raman microspectroscopy versus RBCs visualized using DAB from serial biopsies. A linear regression line has been plotted ($F_{[1,20]}$ = 46.94, $P$ < 0.0005, adjusted $R^2$ = 0.686). NRP120 samples are in red circles. When these are excluded, there is a very strong positive correlation ($F_{[1,16]}$ = 82.17, $P$ < 0.0005, adjusted $R^2$ = 0.835). (D) Number of RBCs per square micrometer at WI45 in the constant blood group (n = 4) is significantly higher than in the blood withdrawal group (n = 7) (Mann-Whitney U test [$P$ = 0.019]).

withdrawal group animals ($P$ = 0.019) (Fig. 4D). The mean number of RBCs per square micrometer of parenchyma in the constant blood group at WI45 (0.0132) was 3 times higher than the mean number of RBCs per square micrometer of parenchyma in the blood withdrawal group (0.00429).

Furthermore, there was a statistically significant positive correlation between hemoglobin content measured using Raman microspectroscopy with 532 nm excitation and the number of DAB-stained RBCs in biopsies from the same specimen (Fig. 4C). However, NRP120 samples do not lie on this regression line; some have a high hemoglobin signal but few DAB-stained RBCs. This supports the hypothesis that some free hemoglobin is present in the liver after erythrocyte lysis and can be detected by the high sensitivity of the Renishaw Raman spectrometer but not DAB stains. When these NRP120 results are excluded, there is a very strong positive correlation ($F_{[1,16]}$ = 82.17, $P$ < 0.0005, adjusted $R^2$ = 0.835).

## SRS MAPS VISUALIZE INDIVIDUAL UNLABELED RBCs IN LIVER PARENCHYMA

Hemoglobin signal may not be from intact RBCs as the liver is responsible for breakdown of erythrocytes, and hemolysis in the extracorporeal circuit is also possible. To determine whether the WI45 increase in Raman signal was primarily due to undamaged erythrocytes, we used SRS to image dewaxed sections of liver parenchyma at high resolution.

SRS uses two lasers to gain information from a single region of the Raman spectrum. This enabled us to take high-resolution Raman images within seconds, rather than hours. Images were obtained at Raman shifts of 1,585 cm$^{-1}$ (peak related to hemoglobin $\nu$[C=C] and $\nu$[C=N] vibrations).[18]

Intact RBCs can be visualized accumulating in constant blood group pigs (Fig. 5), suggesting that the majority of the signal at 1,585 cm$^{-1}$ can be assigned to erythrocytes. They appear as circular, biconcave bright cells with a strong signal at 1,585 cm$^{-1}$. However, RBCs did not accumulate in the blood withdrawal group, where 10% of circulating blood had been removed, apart from in pigs 5 and 8, matching what was seen in stained biopsies (Fig. 6).

## HANDHELD SIGNAL MEASUREMENTS SHOW OPTICAL CHANGES IN LIVERS OVER THE DCD NRP TIME COURSE

To investigate whether optical changes characteristic of liver damage could be measured using a spectrometer suitable for use in the transplant theater, we took measurements over the DCD time course using a simple handheld instrument (Supporting Fig. S4). Porcine liver exhibits an extremely strong non-Raman background signal at 785 nm excitation (near-infrared light) as measured using a CBex handheld Raman spectrometer, due to fluorescence or other non-Raman signal. This can be seen as a large, broad band spanning 400-2,300 cm$^{-1}$ (Supporting Fig. S5).

There was a significant reduction in the total signal obtained using the handheld Raman spectrometer in WI45 livers compared to T0 livers in the LML of all pigs (n = 7) (Fig. 7). In all cases, the total signal then increased between WI45 and NRP120. This suggests that the correlation between congestion and Raman signal observed in isolated biopsies is mirrored by a change in the bulk optical properties of the liver when measured *in situ*. Handheld measurements from the right lateral lobe of the liver showed a less obvious trend, perhaps due to a difference in blood flow (Supporting Fig. S13). This is supported by the observation that the total signal measured was much lower when data were acquired within blood vessels (aorta and vena cava) compared to the surface of the liver parenchyma (Supporting Fig. S6).

# Discussion

The use of marginal liver grafts is on the rise, so accurate assessment of liver health and function is more critical than ever. DCD WI is a complex process, but there are few ways to monitor its effects on organ viability in a noninvasive manner.

Although it is possible to image the liver using noninvasive techniques such as ultrasound, MRI scans, and fluorescence spectroscopy, none of these techniques yield specific biochemical information, leading to limited diagnostic accuracy and insufficient information about liver function. In particular, microvascular damage is difficult to image in an accurate, quantitative manner. Ultrasound is susceptible to

**Constant blood group**
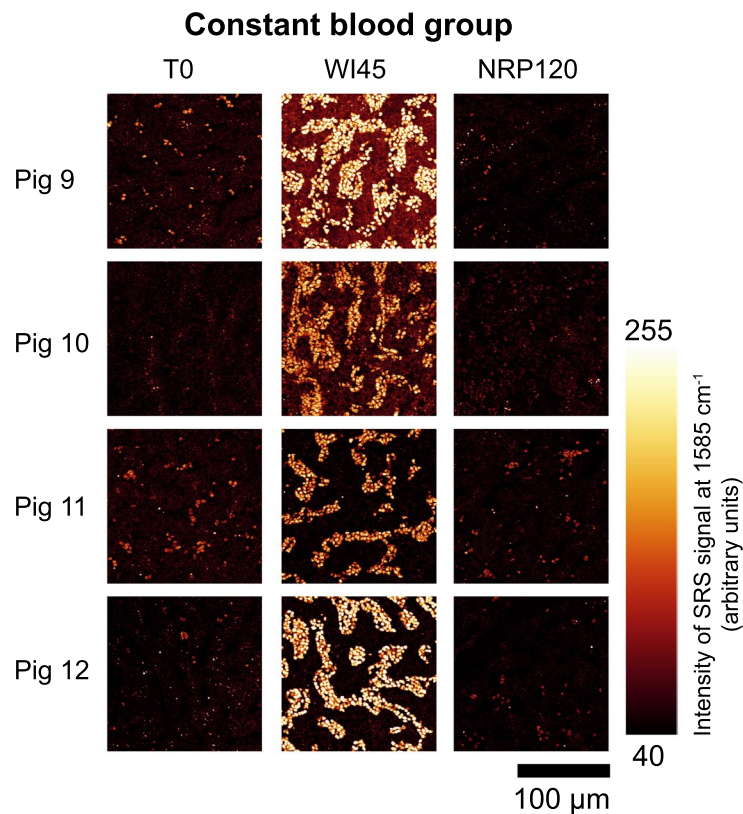


**FIG. 5.** SRS microspectroscopic images of constant blood group liver parenchyma at T0, WI45, and NRP120. In constant blood group animals, no blood was removed prior to circulatory arrest. Formalin-fixed, paraffin-embedded sections (4 µm thick) on glass slides were dewaxed. Images were obtained at a Raman shift of 1,585 cm$^{-1}$ using a Leica Microsystem SP8 multiphoton confocal microscope with a ×25/NA 0.95 HC PL water immersion objective and a CARS 1200S filterwheel. Data were acquired using a 100-mW Stokes (1,032 nm excitation) and a 200-mW pump laser (886.6 nm excitation) with a 227.3 gain, 1,024 × 1,024 resolution, and a line average of 5.

interoperator variability and has low depth penetration and resolution, while MRI scans require large, expensive machines, rendering them unsuitable for the transplant field.[19] Fluorescence spectroscopy, meanwhile, lacks sensitivity and specificity as exogenous fluorescent tracers must be administered prior to imaging, and these have broad emission, which may overlap with intrinsic liver autofluorescence that can fluctuate according to multiple factors.[20]

In contrast, Raman spectroscopy gives quantitative, label-free molecular information. It can be implemented at the micro scale for use in research—as we have demonstrated through high-resolution SRS images—and at the macro scale for use in the clinic—for example, by using a handheld Raman spectrometer.

A number of studies have suggested that RBCs are released into the peripheral liver parenchyma during WI due to microcirculatory failure. This extravasation is associated with damage to liver sinusoidal endothelial cells and poor prognosis.[21,22] However, these studies have relied on stained biopsies or injection of fluorescent dyes and have been limited to rodent models. Moreover, it is unclear how extravasation can be prevented without pharmaceuticals.

Here, we show that erythrocytes accumulate within the peripheral parenchyma during a period of extended WI in a DCD model. By reducing the circulating volume of blood by 10%, extravasation was prevented. Thus, reducing blood volume prior to circulatory arrest could prevent vascular damage and improve organ viability. This finding warrants further research and could influence the transplant procedure.

Furthermore, we can detect RBC accumulation by virtue of the specific, easily identifiable hemoglobin signal in an entirely label-free manner by Raman spectroscopy.
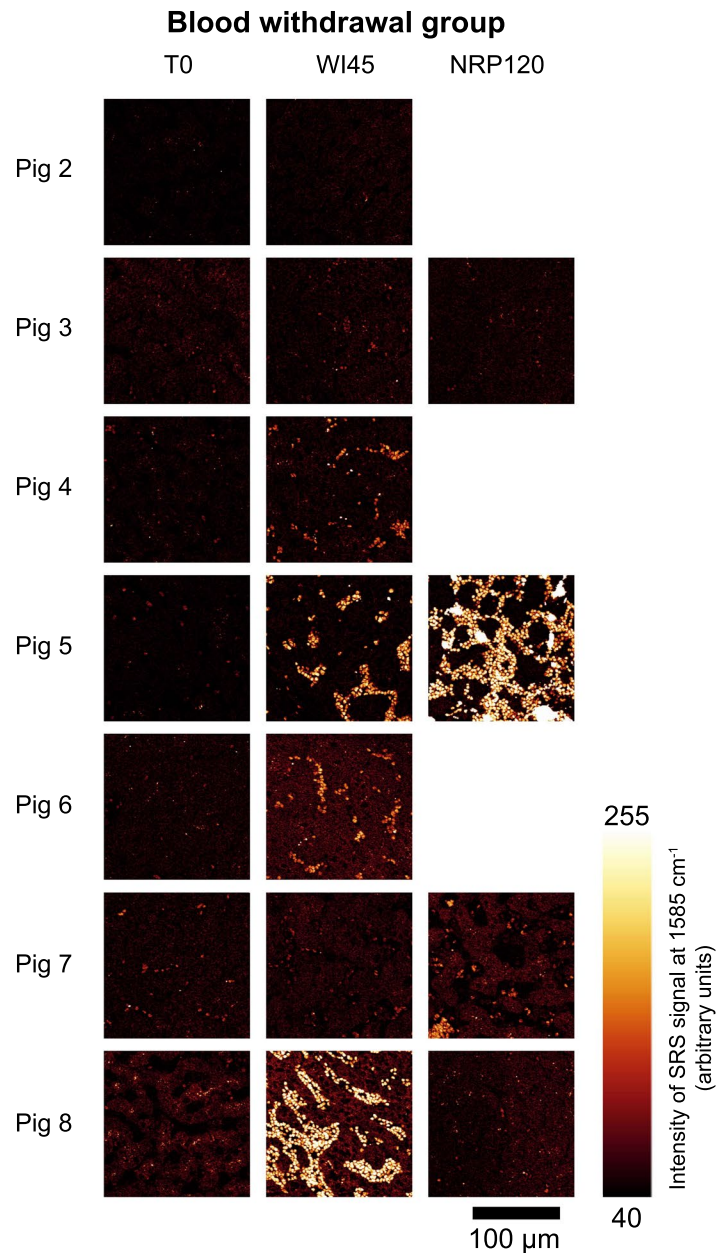
**FIG. 6.** SRS microspectroscopic images of sections of blood withdrawal group liver parenchyma from T0, WI45, and NRP120 biopsies. The blood withdrawal group had 10% of circulating volume of blood removed prior to circulatory arrest. Formalin-fixed, paraffin-embedded sections (4 μm thick) on glass slides were dewaxed. Images were obtained at a Raman shift of 1,585 cm$^{-1}$ using a Leica Microsystem SP8 multiphoton confocal microscope with a ×25/NA 0.95 HC PL water immersion objective and a CARS 1200S filterwheel. Data were acquired using a 100-mW Stokes (1,032 nm excitation) and a 200-mW pump laser (886.6 nm excitation). Images were acquired with a 227.3 gain, 1,024 × 1,024 resolution, and a line average of 5.

We also found that 2 hours of NRP were sufficient to clear the parenchyma of RBCs in all but one pig, suggesting a possible mechanism through which NRP improves posttransplant function and reduces the incidence of ischemic cholangiopathy.[21,22]

## HISTOLOGY

Pathological scoring shows that liver tissue was significantly more injured and congested at WI45 compared to T0 and NRP120 in animals with constant
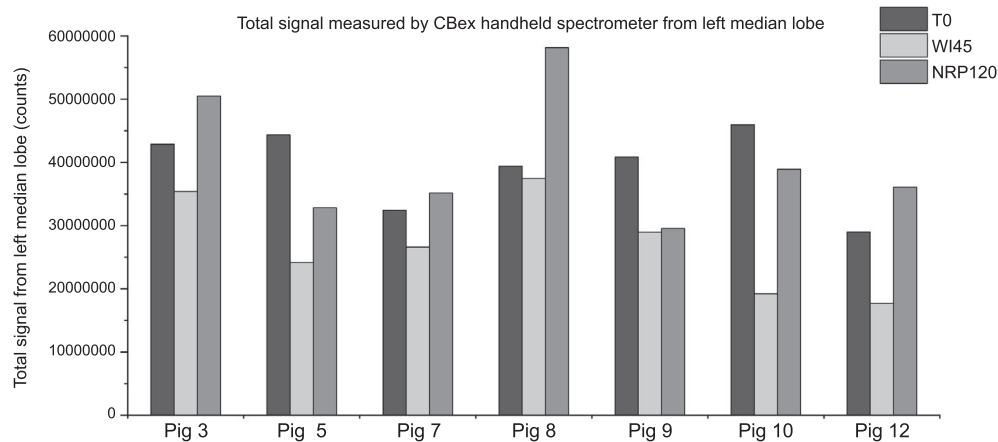
**FIG. 7.** Bar charts showing total signal intensity of *in situ* porcine liver over a DCD time course at T0, WI45, and NRP120. Measurements were taken using a 785-nm CBex handheld Raman spectrometer from the surface of *in situ* liver (10 seconds acquisition, 10.8 mW laser power). (A) Total signal intensity was lower at WI45 compared to T0 and NRP120 in the LML. Repeated measures ANOVA shows this to be statistically significant ($F_{[2,12]}$ = 8.707, $P$ = 0.005).

blood volume (Fig. 2). However, congestion and Suzuki scores were not significantly different in WI45 animals where 10% of circulating blood had been removed. This suggests that reducing blood volume could prevent microvascular damage after circulatory arrest. At NRP120, sinusoidal dilation was apparent in some cases, perhaps due to RBC accumulation.

## LABEL-FREE DETECTION OF RBCs BY RAMAN SPECTROSCOPY

We detected changes in hemoglobin content in liver parenchyma biopsies in a label-free way using Raman microspectroscopy. There was a positive correlation between hemoglobin Raman signal and density of DAB-stained RBCs, measured by linear regression (Figs. 3 and 4). This strongly suggests that RBCs can be detected by their intrinsic Raman hemoglobin signal, a result supported by SRS images obtained by imaging the 1,585 cm$^{-1}$ peak of hemoglobin (Fig. 5). We can therefore differentiate between preischemic and postischemic liver by virtue of hemoglobin in a label-free manner.

It is important to note that Raman spectroscopy seems to detect residual free hemoglobin in NRP120 samples even after RBCs were cleared (Figs. 3 and 4). This is most likely because spectra were obtained with a highly sensitive spectrometer. All severely congested samples yielded a hemoglobin signal >79% (Fig. 3). By

implementing such a sensitivity threshold, Raman spectroscopy could be used to noninvasively detect severe congestion, even where free hemoglobin is present.

## CHANGES IN HEPATIC OPTICAL PROPERTIES IN A CLINICAL SETTING

Significant changes in the optical properties of the left lobe after WI45 can be detected noninvasively using a handheld CBex spectrometer with 785 nm excitation (Fig. 7). These changes were not differences in Raman signal but rather a reduction during ischemia in the strong non-Raman background signal exhibited by bulk liver tissue. RBC accumulation likely overwhelms liver autofluorescence arising from collagen, NADH, and vitamin A. The different responses of the left lateral lobe and right median lobe are possibly due to variations in blood flow. These results are consistent with rat studies in which, although autofluorescence rose in the first 20 minutes of ischemia, liver autofluorescence was reduced compared to basal levels after 1 hour of WI.[20]

## FUTURE WORK AND APPLICATIONS

These results show that Raman spectroscopy can be used to detect biomolecular changes during the

## REFERENCES

1) Organ Procurement and Transplantation Network. U.S. Department of Health and Human Sciences. Current US waiting list by organ type, based on OPTN data as of February 2021. https://optn.transplant.hrsa.gov/data/view-data-reports/national-data/#

2) Kim WR, Lake JR, Smith JM, Skeans MA, Schladt DP, Edwards EB, et al. OPTN/SRTR 2013 annual data report: liver. Am J Transplant 2015;15(Suppl. 2):1-28.

3) Orman ES, Barritt AS, Wheeler SB, Hayashi PH. Declining liver utilization for transplantation in the United States and the impact of donation after cardiac death. Liver Transpl 2013;19:59-68.

4) Organ donation and transplantation: activity report 2017/18. Bristol, UK: NHS Blood and Transplant; 2018.

5) Olthof PB, van Golen RF, Meijer B, van Beek AA, Bennink RJ, Verheij J, et al. Warm ischemia time-dependent variation in liver damage, inflammation, and function in hepatic ischemia/reperfusion injury. Biochim Biophys Acta Mol Basis Dis 2017;1863:375-385.

6) Monbaliu D, van Pelt J, De Vos R, Greenwood J, Parkkinen J, Crabbé T, et al. Primary graft nonfunction and Kupffer cell activation after liver transplantation from non-heart-beating donors in pigs. Liver Transpl 2007;13:239-247.

7) Oniscu GC, Randle LV, Muiesan P, Butler AJ, Currie IS, Perera MT, et al. In situ normothermic regional perfusion for controlled donation after circulatory death—the United Kingdom experience. Am J Transplant 2014;14:2846-2854.

8) Fondevila C, Hessheimer AJ, Ruiz A, Calatayud D, Ferrer J, Charco R, et al. Liver transplant using donors after unexpected cardiac death: novel preservation protocol and acceptance criteria. Am J Transplant 2007;7:1849-1855.

9) Smekal A. [Zur Quantentheorie der Dispersion]. Naturwissenschaften 1923;11:873-875 [in German].

10) Raman CV, Krishnan KS. A new type of secondary radiation. Nature 1928;121:501-502.

11) Smith E, Dent G. Modern Raman Spectroscopy: A Practical Approach. Hoboken, NJ: John Wiley & Sons; 2005.

12) Ember KJI, Hoeve MA, McAughtrie SL, Bergholt MS, Dwyer BJ, Stevens MM, et al. Raman spectroscopy and regenerative medicine: a review. NPJ Regen Med 2017;2:12.

13) Krishna CM, Sockalingum GD, Kegelaer G, Rubin S, Kartha VB, Manfait M. Micro-Raman spectroscopy of mixed cancer cell populations. Vib Spectrosc 2005;38:95-100.

14) Chan JW, Lieu DK, Huser T, Li RA. Label-free separation of human embryonic stem cells and their cardiac derivatives using Raman spectroscopy. Anal Chem 2009;81:1324-1331.

15) Jermyn M, Mok K, Mercier J, Desroches J, Pichette J, Saint-Arnaud K, et al. Intraoperative brain cancer

detection with Raman spectroscopy in humans. Sci Transl Med 2015;7:274ra219.

16) Suzuki S, Toledo-Pereyra LH, Rodriguez FJ, Cejalvo D. Neutrophil infiltration as an important factor in liver ischemia and reperfusion injury. Modulating effects of FK506 and cyclosporine. Transplantation 1993;55:1265-1272.

17) Bankhead P, Loughrey MB, Fernández JA, Dombrowski Y, McArt DG, Dunne PD, et al. QuPath: open source software for digital pathology image analysis. Sci Rep 2017;7:16878.

18) Brunner H, Sussner H. Resonance Raman-scattering on hemoglobin. Biochem Biophys Acta 1973;310:20-31.

19) Sahani DV, Kalva SP. Imaging the liver. Oncologist 2004;9:385-397.

20) Croce AC, Ferrigno A, Santin G, Piccolini VM, Bottiroli G, Vairetti M. Autofluorescence of liver tissue and bile: organ functionality monitoring during ischemia and reoxygenation. Lasers Surg Med 2014;46:412-421.

21) Vollmar B, Glasz J, Leiderer R, Post S, Menger MD. Hepatic microcirculatory perfusion failure is a determinant of liver dysfunction in warm ischemia–reperfusion. Am J Pathol 1994;145:1421-1431.

22) Miyashita T, Nakanuma S, Ahmed AK, Makino I, Hayashi H, Oyama K, et al. Ischemia reperfusion–facilitated sinusoidal endothelial cell injury in liver transplantation and the resulting impact of extravasated platelet aggregation. Eur Surg 2016;48:92-98.

# Supporting Information

Additional Supporting Information may be found at onlinelibrary.wiley.com/doi/10.1002/hep.31701/suppinfo.